Zeitschrift: Eclogae Geologicae Helvetiae
Herausgeber: Schweizerische Geologische Gesellschaft
Band: 97 (2004)
Heft: 1

Artikel: Timing of deglaciation on the northern Alpine foreland (Switzerland)
Autor: Ivy-Ochs, Susan / Schäfer, Jörg / Kubik, Peter W.
DOI: https://doi.org/10.5169/seals-169096

0012-9402/04/010047-9
DOI 10.1007/s00015-004-1110-0
Birkhäuser Verlag, Basel, 2004

Eclogae geol. Helv. 97 (2004) 47–55

Timing of deglaciation on the northern Alpine foreland (Switzerland)

SUSAN IVY-OCHS[1], JÖRG SCHÄFER[2], PETER W. KUBIK[3], HANS-ARNO SYNAL[3] & CHRISTIAN SCHLÜCHTER[4]

Key words: Last glacial maximum, Rhône Glacier, surface exposure dating, cosmogenic isotopes, ^{10}Be, ^{26}Al, ^{36}Cl, ^{21}Ne

ABSTRACT

In order to understand the forcing and the feedback mechanisms working within the climate system knowledge of the timing of cold events across the globe is necessary. This information is especially crucial for the last glacial maximum (LGM) and the subsequent deglaciation. Our approach is to directly date the classical terminal moraines of the Rhône Glacier on the northern Alpine foreland. The Rhône Glacier was the dominant piedmont glacier of the Swiss Alps during the LGM. We have analyzed four erratic blocks from the Wangen a.d. Aare region (near Solothurn) for in-situ cosmogenic ^{10}Be, ^{26}Al, ^{36}Cl and ^{21}Ne. Weighted mean ages based on all radionuclide measurements for each boulder indicate that break down of the Rhône piedmont glacier system occurred between 21.1 and 19.1 ka. The oldest age obtained, 21.1 ka from block ER 1, pinpoints the onset of deglaciation. Pull-back from the Wangen maximum position was complete by no later than 19.1 ka. Reaching of the maximum extent of the Rhône Glacier, during the last glaciation, was contemporaneous with the worldwide ice maximum between 24 and 19 ka.

ZUSAMMENFASSUNG

Das Wissen über die zeitliche Abfolge von Eiszeiten in globalem Massstab ist ein essentielles Element zum Verständnis der Anregungs- und Rückkopplungsmechanismen unseres Klimasystems. Von besonderem Interesse ist das letzte glaziale Maximum (LGM) und der darauffolgende Gletscherrückzug. Unser Beitrag besteht darin, die klassischen Endmoränen des Rhônegletschers im nördlichen Alpenvorland direkt mit der Oberflächen-Expositions-Methode zu datieren. Der Rhônegletscher formte den mächtigsten Vorlandgletscher der Schweizer Alpen während des LGM. Wir analysierten vier erratische Blöcke aus der Region Wangen a.d. Aare (bei Solothurn) auf die folgenden in-situ produzierten kosmogenen Isotope: ^{10}Be, ^{26}Al, ^{36}Cl und ^{21}Ne. Die gewichteten Altersmittel, basierend auf allen Radionuklid-Analysen des jeweiligen Blocks, deuten auf einen Rückzug des Gletschers zwischen 21.1 und 19.1 ka hin. Dabei wird der Beginn des Gletscherrückzugs durch das höchste Alter (21.1 von Block ER 1) angezeigt. Der Rückzug vom Höchststand bei Wangen a.d. Aare war spätestens ca. 19.1 ka vollendet. Der Rhônegletscher erreichte seine Maximalausdehnung während der letzten Eiszeit zeitgleich mit dem weltweiten Eismaximum zwischen 24 und 19 ka.

Introduction

During the maximum of the late Pleistocene glaciation (late Würm), mountain glaciers extended from the Alps, spread out onto the foreland and coalesced into huge piedmont lobes (e.g. Jäckli 1970). Snowline depression in comparison with the modern snowline was approximately 1200 m (Haeberli 1991; Maisch 1982, 1992). The two dominant piedmont glaciers in Switzerland, the Rhône in the west and the Rhine in the east (Fig. 1), remained outside the boundary of the Alps for thousands of years. Lacking direct dating, the length of this interval was estimated based on the morphology of the terminal moraines and the volume of sediment (especially outwash) at the maximum terminal positions (e.g. Penck & Brückner 1901/1909). The sequence of events during disintegration of the piedmont lobes and consequent formation of the numerous foreland lakes (during the Oldest Dryas) has been characterized based on lithostratigraphic, pollen and oxygen isotope data (e.g. Eicher 1987; Furrer 1991; Ammann et al. 1994; Magny 2001). Nevertheless, initiation of ice collapse has never been dated successfully. For the most part, the timing of the deglaciation of the northern Swiss foreland has been based on one radiocarbon date. That date, from Lake Zurich, is 14,600 ± 250 ^{14}C years BP (Lister 1988) and corresponds to a calibrated age range of 17,100-17,850 cal years BP (Stuiver et al. 1998). Questions about when ice in the western Alps attained its maximum extent (cf. Gillespie & Molnar 1995) and when ice collapse began remain.

[1] Institut für Teilchenphysik, ETH Hönggerberg, CH–8093 Zürich, Switzerland
[2] Lamont-Doherty Earth Observatory Palisades, New York 10964 U.S.A.
[3] Paul Scherrer Institut c/o Institut für Teilchenphysik, ETH Hönggerberg, CH–8093 Zürich, Switzerland
[4] Geologisches Institut, Universität Bern, CH–3012 Bern, Switzerland

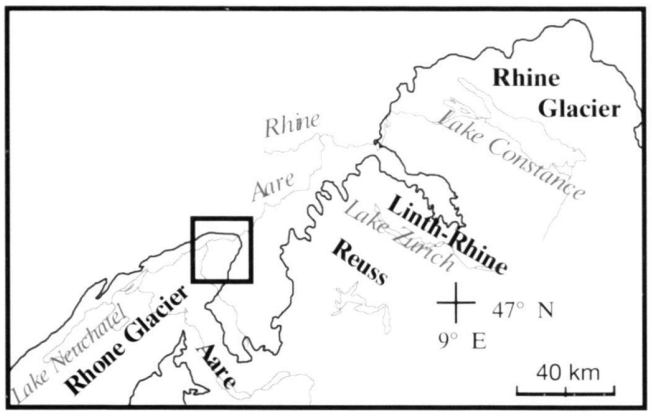

Fig. 1. Location of the study area (highlighted square) with respect to the terminal positions of the major piedmont glaciers north of the Swiss Alps during the LGM (modified from Jäckli 1970). Generalized present-day drainage and the locations of the lakes referred to in the text are shown.

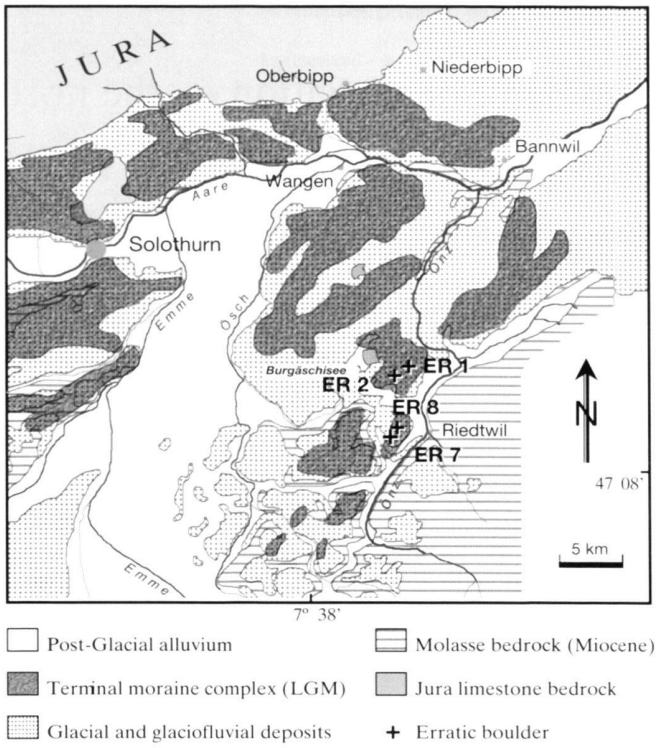

Fig. 2. Schematic map of the Wangen a.d. Aare region. Areas covered by landforms related to the Wangen, Solothurn and Brästenberg stadial moraines are shown in dark grey (based on Nussbaum 1910, 1951; Ledermann 1978). Sampled erratic locations are shown as crosses.

We have attempted to reconstruct the timing of ice decay by surface exposure dating (Lal 1991; Gosse & Phillips 2001) of some of the largest erratic blocks related to the maximum terminal position of the Rhône Glacier during the last glacial maximum (LGM). At this time, the Rhône Glacier was the dominant ice mass in the western Alps. Therefore, constraining the timing of its LGM maximum extension provides basic information about the timing of late Pleistocene glaciation in the Alps. Such data is urgently needed to elucidate crucial thresholds within the Earth's climate system (Alley et al. 2003). We present ^{10}Be ($t_{1/2}$=1510 ka), ^{26}Al ($t_{1/2}$=716 ka), ^{36}Cl ($t_{1/2}$=301 ka) and ^{21}Ne data. ^{10}Be has been analyzed in four boulders, ^{26}Al in three, and ^{36}Cl and ^{21}Ne in one boulder each. By comparing ^{10}Be, ^{26}Al and ^{36}Cl in one rock surface, we have been able to gauge the effect of erosion on the exposure ages (cf. Phillips et al. 1997). Our goal in measuring cosmogenic neon in one boulder was to quantify exposure acquired prior to its deposition at Wangen (cf. Niedermann 2002).

Geologic setting

At the height of the LGM, the Rhône Glacier filled the Rhône Valley and overflowed onto the foreland. Obstructed by the Jura Mountains, the glacier split into a southern (Geneva) and a northern (Solothurn) lobe. The northern lobe, fortified by the contribution of the Aare Glacier, dominated the northern Alpine foreland. It was several hundred kilometers long and up to one kilometer thick (Haeberli 1991). The late Pleistocene maximum terminal equilibrium position was reached near Wangen a.d. Aare (Fig. 2).

The assemblage of moraine and terrace landforms in the region between Solothurn and Wangen has been subdivided into three stadials; Wangen, Solothurn and Brästenberg (Nussbaum 1910, 1951; Furrer 1948; Hantke 1977; Ledermann 1978). The Wangen stadial represents the maximum extent, the Solothurn is defined by the moraine ridges partially encircling Solothurn. The Brästenberg position lies geographically but not necessarily temporally, between the other two stadials. The Brästenberg has been interpreted as evidence for overrunning of some of the Solothurn deposits by the Rhône Glacier (Nussbaum 1910, 1951).

In detail, the left lateral position related to the Wangen stadial consists of sub-parallel moraine ridges skirting the Jura front and flanked in part by kame terraces. The end moraine region (breached by the Aare), grades distally into northeast-dipping glaciofluvial gravels (Niederterrasse). Proximally, drumlin swarms lie in the region north of Burgäschisee (Ledermann 1978). Along the right lateral position, glacial sediments, rarely formed into indistinct flat moraines, drape an uneven bedrock erosional surface cut into the marls and sandstones of the Freshwater Molasse (Miocene). This relict surface is made up of isolated hills of Molasse bedrock separated by dry valleys. It reflects pre-glaciation drainage patterns overprinted by channels formed by meltwater during diversion of the Emme and Aare rivers by the Rhône Glacier (Nussbaum 1910, 1951).

Huge erratic boulders ('Findlinge') once marked the glacier stillstand positions. Their often unusual (i.e. non-local) lithologies contributed to the realization that the Rhône Glacier had once extended hundreds of kilometers outside of the

Alps (de Charpentier 1841). Today very few of the blocks remain; most were destroyed and used for construction material. Even ER 1, the 10 m high erratic discussed here, bears scars of attempts to destroy it with dynamite.

The boulders we sampled were located on the outermost terminal deposits (Wangen stadial). We sampled the flat tops of the boulders using a hammer and chisel. The four largest boulders were analysed. The erratics at Steinhof and Steinenberg are a weakly-foliated hornblende granite ('Arkesin'; Nussbaum 1910). This lithology is characterized by alternating bands of chlorite-talc schist and granitic gneiss. Coarser bands of the latter contain distinctive 1–2 cm long hornblendes (slightly altered to chlorite along the margins), the quartz grains range up to 0.6 mm in size. The blocks likely originated from rockfall onto glaciers (which fed the Rhône Glacier) in the region of Val de Bagnes in Valais (Nussbaum 1910; Ledermann 1978) (see also Kelly et al. 2004).

Analytical procedures

^{10}Be and ^{26}Al were measured in a pure quartz mineral separate produced by selective chemical dissolution (Kohl & Nishiizumi 1992). Be and Al were extracted from the dissolved quartz using standard procedures (Ochs & Ivy-Ochs 1997). Stable Al was measured on an aliquot of the dissolved quartz solution with ICP-OES (inductively-coupled plasma optical emission spectroscopy) using three standard additions for every sample.

The <0.4 mm size fraction (from the same crushed rock used for the ^{10}Be and ^{26}Al) was used for ^{36}Cl sample preparation. Sample preparation for ^{36}Cl generally followed the method of Zreda (1994) and is given in detail in Ivy-Ochs et al. (1996). Before dissolution, the rock powder was leached with HNO_3. No Cl carrier was added in the final dissolution. AgCl was precipitated from the dissolved rock solution. Sulfur was separated with a $BaSO_4$ precipitation step. The following elements were determined commercially by XRAL, Canada: Major elements by XRF; Gd and B by prompt gamma neutron activation; U, Th, and Sm by ICP-MS; and Cl by ion selective electrode (Tab. 1). All were measured on an aliquot of leached rock powder.

^{10}Be/^{9}Be, ^{26}Al/^{27}Al, (Kubik et al. 1998) and ^{36}Cl/Cl (Synal et al. 1997), along with appropriate standards and blanks, were measured by accelerator mass spectrometry at the ETH/PSI tandem facility in Zurich. Chemistry blanks were in the range of 2-3 x 10^{-14} for ^{10}Be/^{9}Be, 3-5 x 10^{-15} for ^{26}Al/^{27}Al, and 5 x 10^{-15} for ^{36}Cl/Cl, yielding contributions of less than 8%, 4% and 1% for ^{10}Be, ^{26}Al and ^{36}Cl, respectively.

For the neon analysis, an ultra-pure quartz separate was handpicked from the chemically-separated quartz used for the radionuclide analysis. The neon analysis followed the protocol given in Bruno et al. (1997). Neon isotopes were analyzed in a non-commercial all-metal magnetic sector mass spectrometer ("Tom Dooley", 90°, 210 mm radius) equipped with a Baur-Signer ion source at the Institute of Isotope Geology and Mineral Resources of the ETH Zurich.

Table 1. Major and minor element concentrations for ER 1.

Element	
SiO_2 (wt. %)	57.8
Al_2O_3 (wt. %)	15.1
Fe_2O_3 (wt. %)	7.27
MnO (wt. %)	0.13
MgO (wt. %)	2.82
CaO (wt. %)	4.62
Na_2O (wt. %)	2.56
K_2O (wt. %)	3.46
TiO_2 (wt. %)	0.9
P_2O_5 (wt. %)	0.18
B (ppm)	7.4
Gd (ppm)	6.6
Sm (ppm)	8
U (ppm)	9.8
Th (ppm)	24.0

Production rates and exposure age calculations

Ages were calculated using the production parameters contained in Tab. 2. Tab. 3 contains the measured neon concentrations, while the measured radionuclide concentrations and calculated exposure ages are listed in Tab. 4. Scaling for latitude (geographic) and altitude for the nucleon component was based on Tab. 2 in Lal (1991). Muon contributions were scaled based on Boezio et al. (2000), Heisinger et al. (2002 a) and Allkofer (1975).

For the ^{36}Cl calculations, using the elemental data in Tab. 1, we have calculated the fraction of thermal neutrons absorbed by the bulk rock to be 0.0054 (after Fabryka-Martin 1988). The correction for sub-surface (non-cosmogenic) production of ^{36}Cl (calculated following Fabryka-Martin 1988) was less than 3%.

No shielding corrections were required except for ER 2, which had a surface dip of 48°. We have made no correction for snow cover. No correction has been made for shielding by forest cover, a rough calculation indicates this would have been less than 1%. No correction has been made for past changes in magnetic field intensity, because during this period at this latitude the correction amounts to less than 1% (Masarik et al. 2001).

Fig. 3 shows the neon three-isotope plot of the data from ER 7. Within the uncertainties, the neon released at all steps was indistinguishable from atmospheric composition (see also Tab. 3). This was expected given the low altitude and short exposure time of the boulder. However, the neon data strongly contradict an overall exposure period (i.e. pre-exposure) of more than approximately 40 ka for ER 7. This suggests that the block had a simple and continuous exposure history since it was deposited by the Rhône Glacier.

Exposure age vs. erosion rate

By measuring ^{36}Cl, in addition to ^{10}Be and ^{26}Al in the same rock surface (ER 1), we have taken a step towards constraining the amount of rock surface weathering (here termed erosion) during

Table 2. Sea level high latitude production rates used for age calculations.

Cosmogenic Isotope	Production Rate	Reference
^{10}Be	atoms (g SiO_2)$^{-1}$ year^{-1}	
spallation	5.28 ± 0.28	Kubik et al. 1998 Kubik & Ivy-Ochs 2004
fast muons	0.093	Heisinger et al. 2002a, 2002b
stopped negative muons	0.106	Heisinger et al. 2002a, 2002b
^{26}Al	atoms (g SiO_2)$^{-1}$ year^{-1}	
spallation	33.9 ± 1.97	Kubik et al. 1998 Kubik & Ivy-Ochs 2004
stopped negative muons	0.814	Heisinger et al. 2002a, 2002b
fast muons	0.697	Heisinger et al. 2002a, 2002b
^{36}Cl		
From Ca	atoms (g Ca)$^{-1}$ year^{-1}	
spallation	48.8 ± 3.4	Stone et al. 1996
muon capture	5.2 ± 1.0	Stone et al. 1998
From K	atoms (g K)$^{-1}$ year^{-1}	
spallation	161 ± 9	Evans 2001
muon capture	10.2 ± 1.3	Evans 2001
From Ti	13.5 atoms (g Ti)$^{-1}$ year^{-1}	Masarik 2002
From Fe	6.75 atoms (g Fe)$^{-1}$ year^{-1}	Masarik 2002
Thermal neutron flux	626 neutrons (g air)$^{-1}$year^{-1}	Phillips et al. 2001
^{21}Ne	atoms (g SiO_2)$^{-1}$ year^{-1} 20.4 ± 3.9	Niedermann 2000

*Calculated from data in Kubik et al. (1998) using an exponential depth profile.

Table 3. Neon data for ER 7.

Step (Temp [°C]/time [minutes])	^{20}Ne (10^9 at/g)	^{21}Ne/^{20}Ne (10^{-3})	^{22}Ne/^{20}Ne (10^{-1})
1 (350/90)	4.28 ± 0.03	2.976 ± 0.174	1.016 ± 0.014
2 (800/35)	10.26 ± 0.06	2.969 ± 0.106	1.016 ± 0.010
Cosmo.: step 1&2	14.54 ± 0.07	2.971 ± 0.093	1.016 ± 0.011
3 (1700/15)	5.92 ± 0.03	2.939 ± 0.120	1.013 ± 0.079

Notes: Neon data for ER 7 given with 1σ confidence level, including statistical, sensitivity and mass-discrimination errors. Errors due to uncertainties of calibration gas amounts are not included but should be <3%. We analyzed 1.0283 g of a handpicked, ultra-pure quartz separate and performed a step-wise heating procedure following Niedermann (2002). The cosmogenic step plotted in Fig. 3 is composed of both the 350 °C and the 800 °C steps. The ^{21}Ne/^{20}Ne ratio of the cosmogenic step is slightly higher than the atmospheric value of 2.959 x 10^{-3}, however uncertainties are too high to unequivocally identify a cosmogenic ^{21}Ne excess.

Table 4. AMS-measured ^{10}Be, ^{26}Al and ^{36}Cl concentrations, calculated no-erosion and 3 mm/ka erosion-corrected exposure ages.

Boulder No.	Alt. (m)	Height (m)	Thick. (cm)	Al (Cl) ppm	Isotope	10^4 atoms/g	no-erosion exposure age (ka)	Mean age (ka)	3 mm/ka exposure age (ka)	Erosion-corr. Mean age (ka)
ER 1	580	10	6		^{10}Be	16.5 ± 1.0	18.9 ± 1.5	20.2	19.9 ± 1.6	21.1
				293	^{26}Al	116 ± 7	20.7 ± 1.8		21.9 ± 1.9	
				(62)	^{36}Cl	30.2 ± 1.4	21.9 ± 2.0		22.0 ± 2.0	
ER 2	585	2.5	5		^{10}Be	15.5 ± 0.7	19.4 ± 1.3	19.4	20.5 ±1.4	20.5
ER 7	610	1	4		^{10}Be	14.3 ± 1.0	15.8 ± 1.3	16.1	16.4 ± 1.3	16.8
				12	^{26}Al	95.6 ± 5.1	16.4 ± 1.3		17.1 ± 1.3	
ER 8	595	1.5	3		^{10}Be	16.2 ± 1.0	17.9 ± 1.4	18.2	18.8 ± 1.5	19.1
				67	^{26}Al	107 ± 5	18.5 ± 1.4		19.4 ± 1.4	

Notes: AMS measurement errors are at the 1σ level, including the statistical (counting) error and the error due to the normalization to the standards and blanks. Exposure age errors include the production rate errors given in Tab. 2, but do not include errors due to latitude and altitude scaling. The overall uncertainty of a given exposure age should be less than 15% (see also Gosse & Phillips 2001).

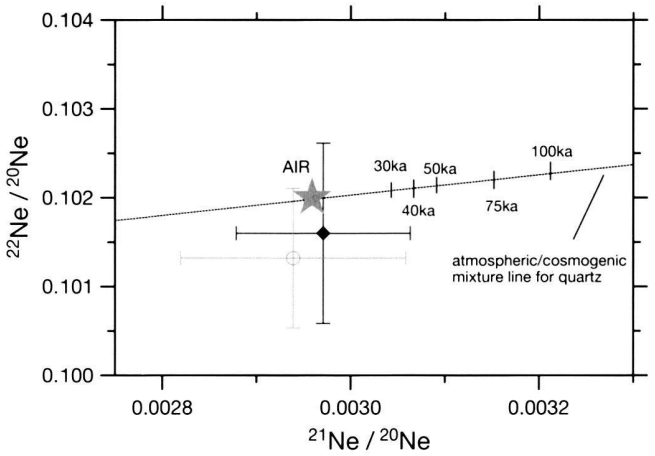

Fig. 3. Neon 3-isotope plot for the sample ER 7. The "cosmogenic" step (composed of two degassing steps, 350 °C, 800 °C) is plotted as black rectangle, the final extraction step (1700 °C) is shown in grey. Both steps plot within uncertainties (1σ) on the atmospheric point (´), i.e. no meaningful cosmogenic neon age can be calculated from this sample. The lines crossing the "atmospheric/cosmogenic mixture line for quartz" labeled with virtual ages from "+30 ka" to "+100 ka" indicate the measured $^{21}Ne/^{22}Ne$-ratio with several virtual cosmogenic ^{21}Ne concentrations added corresponding to virtual exposure periods. The addition of virtual exposure ages of 30 ka and 40 ka still plot within the error bars. However, the addition of a virtual exposure age of more than 40 ka moves the $^{21}Ne/^{22}Ne$-ratio outside of the error bar. The Ne data for sample ER 7 is consistent with exposure ages of up to, but contradicts a pre-exposure period of more than, 40 ka.

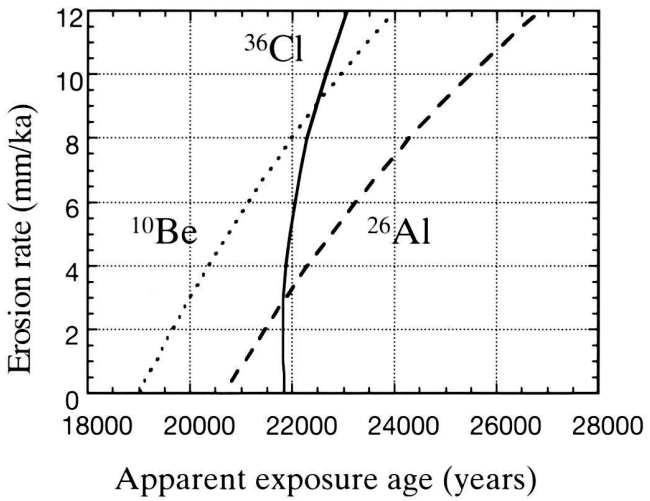

Fig. 4. Plot of erosion rate vs. apparent exposure age based on the measured concentrations of ^{10}Be, ^{26}Al and ^{36}Cl from ER 1 (Tab. 4). All production parameters for this figure are listed in Tab. 2. We followed the method of calculation outlined in Dep et al. (1994, 1997) and Liu et al. (1994) (see also Phillips et al. 1997; Gosse & Phillips 2001). The shape of the ^{36}Cl curve differs from the other two because it is produced by thermal neutron capture in addition to spallation. Where a given line crosses the x-axis shows the apparent exposure age calculated with no erosion. The point at which the ^{10}Be (or ^{26}Al) line crosses the ^{36}Cl line indicates both erosion rate and exposure age corresponding to the measured concentrations. Erosion rates determined using either ^{10}Be or ^{26}Al are in agreement when considering the uncertainties.

the exposure period (Phillips et al. 1997; Gosse & Phillips 2001). In Fig. 4, erosion rate is plotted vs. apparent exposure age for each of the three isotopes using the ER 1 data (Tab. 1 and 3) and the production rates of Tab. 2. The erosion rate vs. exposure age lines for ^{10}Be and ^{26}Al were calculated based on the equations in Lal (1991). For ^{36}Cl, we followed the calculation method outlined in Liu et al. (1994) (see also Dep et al. 1994, 1997).

^{10}Be and ^{26}Al are produced predominantly by spallation, that means that production decreases with depth. For these isotopes, the effect of weathering or erosion on the rock surface is to remove the outermost part which contains the highest concentrations of cosmogenic isotopes. As the rate of erosion increases, the difference between 'true' exposure age and apparent exposure age (calculated assuming no erosion) increases. The 'true' ^{10}Be or ^{26}Al exposure age is always older.

In contrast, ^{36}Cl is also produced by thermal neutron capture (Gosse & Phillips 2001 and references therein). Thermal neutrons can escape back out of a surface, which means that the maximum production of ^{36}Cl occurs not at the rock surface but at a depth of approximately 20 cm in the rock (Fabryka-Martin 1988). Furthermore, the shape of the ^{36}Cl depth curve is controlled by the proportion of production coming from thermal neutron capture, which is in turn dependent on rock composition. As a seen in Fig. 4, for ER 1, the erosion rate vs. exposure age line for ^{36}Cl is much steeper than for ^{10}Be or ^{26}Al. That means that the effect of erosion on the ^{36}Cl exposure age is much less than for ^{10}Be or ^{26}Al.

Examination of the point where the ^{10}Be (or ^{26}Al) line crosses the ^{36}Cl line (Fig. 4) can reveal the erosion rate for ER 1. This method yields 9 mm/ka based on ^{10}Be and 3 mm/ka based on ^{26}Al. These values fit with estimates based on the appearance of the rock surface. The height of more resistant quartz-rich areas above the surrounding rock is less than 6 cm. If one assumes a 20 ka exposure period, one obtains an erosion rate of 3 mm/ka. To be consistent with both the rock surface appearance and the information gleaned from Fig. 4, we have conservatively chosen to use an erosion rate of 3 mm/ka to calculate erosion-corrected ages. For comparison, we note that erosion rates for granite and granodiorite boulders in Wyoming determined by Phillips et al. (1997) are 2.4 mm/ka or less. While Small et al. (1997) found erosion rates of up to 7 mm/ka for granitic bedrock tors at four Rocky Mountain sites. We present both uncorrected and erosion-corrected exposure ages in Tab. 4. In the following discussion, we use the erosion-corrected ages but the overall conclusions in no way hinge upon this choice.

Interpretation of the exposure ages

Construction of a moraine by a valley glacier can occur relatively rapidly (tens to hundreds of years), while a piedmont lobe may fluctuate at its maximum terminal position for thousands of years. Either glacier can be visualized as pushing slightly forward some years and melting back a little bit some

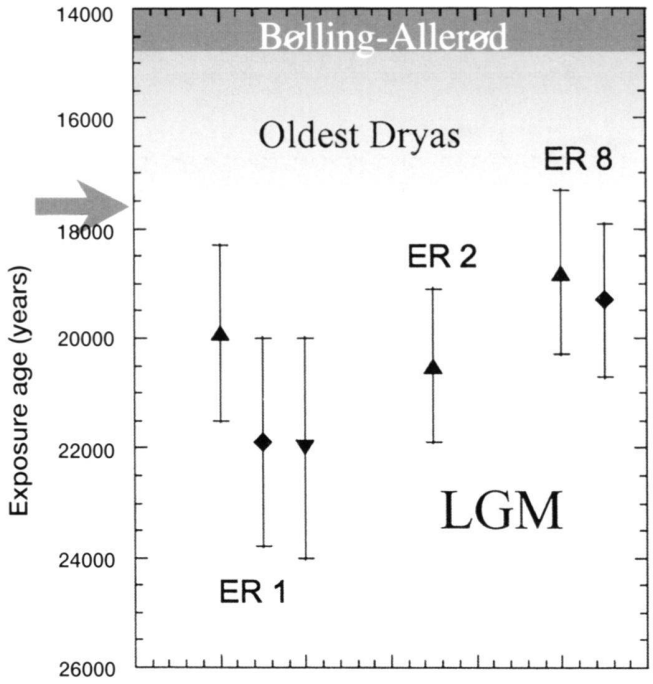

Fig. 5. Plot of erosion-corrected exposure ages for boulders ER 1, ER 2, and ER 8. ^{10}Be ages are shown with a triangle, ^{26}Al ages with a diamond, ^{36}Cl ages with an upside down triangle. The arrow indicates the point for the earliest likely formation of the foreland lakes (ca. 17.5 ka). The beginning of the Oldest Dryas in northern Switzerland has not been strictly defined, therefore its lower boundary is shown shaded.

years. During a brief advance, slightly older deposits can be overridden. Barring post-depositional effects, the exposure age represents the length of time since the boulder (and by inference the moraine) stabilized following glacier retreat (cf. Zreda & Phillips 1995; Phillips et al. 1997; Gosse & Phillips 2001). A recent statistical study (Putkonen & Swanson 2003), which included most published exposure ages from boulders on moraines, found that the oldest age obtained is generally within 10% of the 'true' age of the deposit (but is nevertheless younger than the 'true' age). The implication is that 1) taking the average of exposure ages obtained from several boulders on a single landform may yield an age which has no glacial-geological meaning, and 2) given that the 'too young' effect is due to weathering, exhumation or general instability of boulders, the difference between 'true' age and apparent exposure age will be greater for older deposits (depending on the nature of the deposit and the local climate).

With these caveats in mind, we conclude that 21.1 ka represents the time at which the Rhône Glacier reached its maximum terminal position during the late Pleistocene. This is based on the error-weighted mean of the ^{10}Be, ^{26}Al and ^{36}Cl erosion-corrected exposure ages for ER 1 (Tab. 4). With our data it is not possible to constrain the earliest time at which the ice reached the Wangen position. But we found neither geomorphologic nor stratigraphic evidence to indicate that stabilization of boulder ER 1 occurred significantly later than the initial glacier advance to Wangen. None of the boulders we dated was overridden during subsequent fluctuations. We interpret the age 19.1 ka from ER 8 to indicate the time when the Rhône Glacier completely withdrew from the Wangen position. Therefore, the Rhône Glacier extended as far as the region of Wangen between 21.1 ka and 19.1 ka. A two thousand year period is consistent with estimates that a several thousand year long stillstand was required for the volume of sediment in the Wangen region to accumulate (Nussbaum 1910, 1951). A similar period was needed to reach the level of erosion observed in the ice-marginal valleys (e.g. Önztal; Ledermann 1978). The age obtained from ER 7 (16.8 ka) has not been included in our discussion. Its age is unreasonably young in comparison to the independent data which indicate an ice-free foreland no later than 17.10–17.85 ka (see also below).

Timing of deglaciation on the northern Alpine foreland

Ice domes built-up in the Alps to the extent (Florineth & Schlüchter 1998, 2000) that glaciers expanded onto the foreland after 28 ^{14}C ka (Furrer 1991; Schlüchter & Röthlisberger 1995). In the eastern part of the northern foreland, the Rhine Glacier had advanced past Chur by 25 ka (Keller 1994). The Rhine, Linth and eventually Reuss Glaciers coalesced to form a huge piedmont lobe that extended from Zurich to Schaffhausen (Fig. 1). Study of sediment cores from Lake Constance has allowed a glimpse at events which took place during and after the collapse of the Rhine Glacier system (Wessels 1998 a, 1998 b). The transition from proglacial varves, with deformed sediment, to deglacial loess deposits (indicating ice-free but also vegetation-free conditions) was set at 17.5 cal ka (Wessels 1998 a, 1998 b). This date is based on correlation with Lake Zurich cores (Niessen et al. 1992) where the end of glacial meltwater influence on δ^{18}O was dated at 14.60 ^{14}C ka (Lister 1988), corresponding to 17.10–17.85 cal ka (Stuiver et al. 1998).

Our ^{10}Be, ^{26}Al and ^{36}Cl exposure dates show that the Rhône Glacier reached Wangen no later than 21.1 ka. It fluctuated at the Wangen position until 19.1 ka (Fig. 5). This interpretation complements those based on δ^{18}0 (Eicher 1979, 1987) and pollen data (Welten 1982) from nearby Burgäschisee (Fig. 2), which indicate that the lake formed during the early part of the Oldest Dryas (cf. Ammann et al. 1994). Farther upstream on the northern end of Lake Neuchâtel, pollen and macrofossil data indicate that the lake basin became ice-free during the earliest phase of the Oldest Dryas (Magny et al. 2003; Hadorn et al. 2002). The oldest radiocarbon date obtained from the Hauterive/Rouges-Terres site (14.25 ± 95 ^{14}C ka; equivalent to 16.8 to 17.4 cal ka, Stuiver et al. 1998) came from material found within the lower zone of the Oldest Dryas (Hadorn et al. 2002), but notably, was not from the base of the core. The Rhône Glacier must have already collapsed by 16.8 to 17.4 ka. Similarly, pollen analyses from numerous foreland lakes confirm that the foreland was completely free of ice during the Oldest Dryas (e.g. Ammann

et al. 1994; Wohlfarth et al. 1994; Magny 2001). This compression of time between retreat of the piedmont glaciers and onset of deposition of lake sediments is consistent with the idea that the massive LGM glaciers collapsed rapidly rather than melted down slowly (Schlüchter 1988; van Husen 1997, 2000).

How then does the timing of events along the northern foreland of the Alps relate to events further afield during the LGM and during the subsequent deglaciation? The build-up of ice volume worldwide had a clear impact on sea level around 30 ka (Lambeck et al. 2002). Ice cores reveal that the lowest temperature in Greenland during the LGM occurred around 24 ka (e.g. Stuiver & Grootes 2000; Johnsen et al. 2001). A barely perceptible rise in sea level set-in just after 21 ka (Hanebuth et al. 2000), but for the most part there was little change in eustatic sea level between 22 ka and 19 ka (Lambeck et al. 2002). The peak of the LGM has been placed temporally between 24 and 19 ka (cf. Clark & Mix 2000; Mix et al. 2001; Clark 2002; Alley et al. 2003). Our exposure dates show that the maximum ice extent of the Rhône Glacier during the late Pleistocene was reached at or slightly before 21.1 ka, thus contemporaneous with the time when continental ice sheets were at their maximum. Rapid rise in sea level right around 19 ka signals the onset of a stronger warming trend (Yokoyama et al. 2000; Clark & Mix 2000; Lambeck et al. 2002). Decay of the British Ice Sheet, as early as 19 ka, reflects this pre-Bølling early deglacial phase (Lagerklint & Wright 1999; Clark 2002) which clearly preceded Heinrich event 1 (McCabe & Clark 1998; Zaragosi et al. 2001). In contrast, the main warming signal in Greenland ice cores is not recorded until the Oldest Dryas/Bølling transition around 14.7 ka (e.g. Alley & Clark 1999; Walker et al. 1999; Stuiver & Grootes 2000). The Rhône Glacier abandoned its maximum position no later than 19.1 ka. Therefore, Alpine piedmont glaciers had abandoned their maximum positions in response to the early phase of deglaciation (cf. Denton et al. 1999; Clark 2002), much like the British Ice Sheet. Alpine glaciers expanded and reached their late Pleistocene maximum terminal positions in concert with the huge continental ice sheets. But because of their sensitivity to minor changes in snowline, they responded more rapidly and collapsed suddenly at the first warming pulse which signaled the onset of deglaciation.

Acknowledgements

We thank K. Fifield, H. Kerschner, M. Maisch and R. Wieler for insightful discussions and critical reviews of an earlier version of this manuscript. Reviews by F. von Blanckenburg and D. van Husen are sincerely appreciated. T. Bingham Müller kindly improved the wording and clarity. We thank J. Beer for use of lab space at EAWAG, S. Bollhalder for help with ^{36}Cl sample preparation and D. Kistler for use of the ICP-OES at EAWAG. Our tandem crew provided faithful technical support. Major and trace element concentrations were measured by XRAL Ontario, Canada. This research was funded by ETH research grant 0-20-624-92 and Swiss National Science foundation grant 21-28971.90. The Zurich AMS facility is jointly operated by the Swiss Federal Institute of Technology, Zurich, and Paul Scherrer Institute, Villigen, Switzerland.

REFERENCES

Allkofer, O.C. 1975: Introduction to Cosmic Radiation. Buchreihe d. Atomenergie Bd 10, Verlag Karl Thiemig, Munich.

Alley, R.B. & Clark, P.U. 1999: The deglaciation of the Northern Hemisphere: A Global Perspective. Earth and Planet. Sci. Lett. 27, 149–182.

Alley, R.B., Marotzke, J., Nordhaus, W.D., Overpeck, J.T., Peteet, D.M., Pielke, R.A., Pierrehumbert, R.T., Rhines, P.B., Stocker, T.F., Talley, L.D. & Wallace, J.M. 2003: Abrupt climate change. Science 299, 2005–2010.

Ammann, B., Lotter, A.F., Eicher, U., Gaillard, M.-J., Wohlfarth, B., Häberli, W., Lister, G., Maisch, M., Niessen, F. & Schlüchter, C. 1994: The Würmian Late-glacial in lowland Switzerland. J. Quaternary Sci. 9, 119–125.

Boezio, M., Carlson, P., Francke, T., Weber, N., Suffert, M., Hof, M., Menn, W., Simon, M., Stephens, S. A., Bellotti, R., Cafagna, F., Circella, M., De Marzo, C., Finetti, N., Papini, P., Piccardi, S., Spillantini, P., Ricci, M., Casolino, M., De Pascale, M. P., Morselli, A., Picozza, P., Sparvoli, R., Barbiellini, G., Schiavon, P., Vacchi, A., Zampa, N., Grimani, C., Mitschell, J.W., Ormes, J.F., Streitmatter, R.E., Bravar, U., Golden, R.L., Stochaj, S.J. 2000: Measurement of the flux of atmospheric muons with the CAPRICE94 apparatus. Phys. Rev. D62 032007, 1–15.

Bruno, L.A., Baur, H., Graf, T., Schlüchter, C., Signer, P. & Wieler, R. 1997: Dating of Sirius Group tillites in the Antarctic Dry Valleys with cosmogenic ^{3}He and ^{21}Ne. Earth and Planet. Sci. Lett. 147, 37–54.

Charpentier, J., de. 1841: Essai sur les glaciers et sur le terrain erratique du bassin du Rhône. Lausanne, 363 p.

Clark, P.U. 2002: Early deglaciation in the tropical Andes. Science 298, 7a.

Clark, P.U. & Mix, A.C., 2000: Ice sheets by volume. Nature 406, 689–690.

Denton, G.H., Lowell, T.V., Heusser, C.J., Moreno, P.I., Andersen, B.G., Heusser, L. E. & Schlüchter, C. 1999: Interhemispheric linkage of paleoclimate during the last glaciation. Geogr. Annaler 81A, 107–153.

Dep, L., Elmore, D. Lipschutz, M., Vogt, S., Phillips, F.M., Zreda, M. 1994: Depth dependence of cosmogenic neutron-capture-produced ^{36}Cl in a terrestrial rock. Nuclear Instr. Meth. B 92, 301–307.

Dep, L., Elmore, D. Vogt, S.T., Sharma, P., Bourgeois, M. & Dunne, A. 1997: Erosion corrected ages of Quaternary geomorphic events using cosmogenic ^{36}Cl in rocks. Purdue University report PL-9703, 13 p.

Eicher, U. 1979: Die ^{18}O/^{16}O und ^{13}C/^{12}C-Isotopenverhältnisse in spätglazialen Süsswasserkarbonaten und ihr Zusammenhang mit den Ergebnissen der Pollenanalyse. Diss. Univ. Bern, 203 p.

Eicher, U. 1987: Die spätglazialen sowie die frühpostglazialen Klimaverhältnisse im Bereiche der Alpen: Sauerstoffisotopenkurven kalkhaltiger Sedimente. Geographica Helv. 2, 99–104.

Evans, J. 2001: Calibration of the production rates of cosmogenic ^{36}Cl from Potassium. Ph.D. diss. Australian National Univ. Canberra, 142 p.

Fabryka-Martin, J.T. 1988: Production of radionuclides in the earth and their hydrogeologic significance, with emphasis on chlorine-36 and iodine-129. Ph.D. diss. University of Arizona, Tucson, 400 p.

Florineth, D. & Schlüchter, C. 1998: Reconstructing the Last Glacial Maximum (LGM) ice surface geometry and flowlines in the Central Swiss Alps. Eclogae geol. Helv. 91, 391–407.

Florineth, D. & Schlüchter, C. 2000: Alpine evidence for atmospheric circulation patterns in Europe during the Last Glacial Maximum. Quaternary Res. 54, 295–308.

Furrer, G. 1991: 25,000 Jahre Gletschergeschichte. Veröff. Naturf. Ges. Zürich, Njbl. 1991, 52 p.

Furrer, H. 1948: Das Quartär zwischen Solothurn und Wangen a. A. Eclogae Geol. Helv. 41, 269–284.

Gillespie, A. & Molnar, P. 1995: Asynchronous maximum advances of mountain and continental glaciers. Rev. Geophys. 33, 311–364.

Gosse, J.C. & Phillips, F.M. 2001: Terrestrial in situ cosmogenic nuclides: theory and application. Quaternary Sci. Rev. 20, 1475–1560.

Haeberli, W. 1991: Zur Glaziologie der letzteiszeitlichen Alpenvergletscherung. In: Klimageschichtliche Probleme der letzten 130000 Jahre (Ed. by Frenzel, B.). Paleoklimaforschung 1, 409–419.

HADORN P., THEW, N., COOPE, G.R., LEMDAHL, G., HAJDAS, I. & BONANI, G. 2002: A Late-Glacial and early Holocene environment and climate history for the Neuchâtel region (CH). In: RICHARD, H & VIGNOT (Eds.): Equilibres et Ruptures dans les Ecosystèmes depuis 20 000 ans en Europe de l'Ouest. Collection Annales Littér. Sér. Environment, Sociétés et Archéologie No. 3, 75–90.

HANEBUTH T., STATTEGGER K. & GROOTES, P.M. 2000: Rapid flooding of the Sunda Shelf: A late-glacial sea-level record. Science 288, 1033–1035.

HANTKE, R. 1977: Eiszeitliche Stände des Rhone-Gletschers im westlichen Schweizer Mittelland. Ber. der Natf. Ges. Freiburg i. Breisgau. 67, 75–83.

HEISINGER, B., LAL, D., JULL, A.J.T., KUBIK, P., IVY-OCHS, S., NEUMAIER, S., KNIE, K., LAZAREV, V. & NOLTE, E. 2002 a: Production of selected cosmogenic radionuclides by muons: 1. Fast muons. Earth and Planet. Sci. Lett. 200, 345–355.

HEISINGER, B., LAL, D., JULL, A.J.T., KUBIK, P., IVY-OCHS, S., KNIE, K. & NOLTE, E. 2002 b: Production of selected cosmogenic radionuclides by muons: 2. Capture of negative muons. Earth and Planet. Sci. Lett. 200, 357–369.

IVY-OCHS, S., SCHLÜCHTER, C., KUBIK, P.W., SYNAL, H.-A., BEER, J. & KERSCHNER, H. 1996: The exposure age of an Egesen moraine at Julier Pass measured with ^{10}Be, ^{26}Al and ^{36}Cl. Eclogae geol. Helv. 89, 1049–1063.

JÄCKLI, A. 1970: Die Schweiz zur letzten Eiszeit: Atlas der Schweiz 6. Eidg. Landestopogr., Wabern-Bern.

JOHNSEN, S.J., DAHL-JENSEN, D., GUNDESTRUP, N., STEFFENSEN, J.P., CLAUSEN, H.B., MILLER, H., MASSON-DELMOTTE, V., SVEINBJÖRNSDOTTIR, A.E. & WHITE, J. 2001: Oxygen isotope and palaeotemperature records from six Greenland ice-core stations: Camp Century, Dye-3, GRIP, GISP2, Renland and NorthGRIP. J. of Quaternary Sci. 16, 299–307.

KELLER, O. 1994: Entstehung und Entwicklung des Bodensees – ein geologischer Lebenslauf. In: Umweltwandel am Bodensee (Ed. by MAURER, H.). UVK, St. Gallen, 33–92.

KELLY, M.A., BUONCRISTIANI, J.-F. & SCHLÜCHTER C. 2004: A reconstruction of the last glacial maximum (LGM) ice-surface geometry in the western Swiss Alps and contiguous Alpine regions in Italy and France. Eclogae geol. Helv. (in press).

KOHL, C.P. & NISHIIZUMI, K. 1992: Chemical isolation of quartz for measurement of in-situ produced cosmogenic nuclides. Geochim. Cosmochim. Acta 56, 3583–3587.

KUBIK, P.W. & IVY-OCHS, S. 2004: A re-evaluation of the ^{10}Be production rate for exposure dating obtained from the Köfels (Austria) landslide. Nuclear Instr. Meth. B (in press).

KUBIK, P.W., IVY-OCHS, S., MASARIK, J., FRANK, M. & SCHLÜCHTER, C. 1998: ^{10}Be and ^{26}Al production rates deduced from an instantenous event within the dendro-calibration curve, the landslide of Köfels, Ötz Valley, Austria. Earth and Planet. Sci. Lett. 161, 231–241.

LAGERKLINT, I.M. & WRIGHT, J.D. 1999: Late glacial warming prior to Heinrich event 1: The influence of ice rafting and large ice sheets on the timing of initial warming. Geology 27, 1099–1102.

LAL, D. 1991: Cosmic ray labeling of erosion surfaces: in situ nuclide production rates and erosion models. Earth and Planet. Sci. Lett. 104, 424–439.

LAMBECK, K., YOKOYAMA, Y. & PURCELL, T. 2002: Into and out of the Last Glacial Maximum: sea-level change during Oxygen Isotope Stages 3 and 2. Quaternary Sci. Rev. 21, 343–360.

LEDERMANN, H. 1978: Geologischer Atlas der Schweiz, Atlasblatt 72 (1127 Solothurn), mit Erläuterungen. Schweiz. Geol. Komm., Bern, 36 p.

LISTER, G.S. 1988: A 15,000-year isotopic record from Lake Zürich of deglaciation and climatic change in Switzerland. Quaternary Res. 29, 129–141.

LIU, B., PHILLIPS, F.M., FABRYKA-MARTIN, J.T., FOWLER, M.M. & STONE, W.D. 1994: Cosmogenic ^{36}Cl accumulation in unstable landforms, 1. Effects of the thermal neutron distribution. Water Resour. Res. 30, 3115–3125.

MAGNY, M. 2001: Palaeohydrological changes as reflected by lake-level fluctuations in the Swiss Plateau, the Jura Mountains and the northern French Pre-Alps during the Last Glacial-Holocene transition: a regional synthesis. Global and Planet. Change 30, 85–101.

MAGNY, M., THEW, N. & HADORN, P. 2003: Late-glacial and early Holocene changes in vegetation and lake-level at Hauterive/Rouges-Terres, Lake Neuchâtel (Switzerland). J. Quaternary Sci. 18, 31–40.

MAISCH, M. 1982: Zur Gletscher- und Klimageschichte des alpinen Spätglazials. Geographica Helv. 37, 93–104.

MAISCH, M. 1992: Die Gletscher Graubündens. Rekonstruktion und Auswertung der Gletscher und deren Veränderungen seit dem Hochstand von 1850 im Gebiet der östlichen Schweizer Alpen (Bündnerland und angrenzende Regionen). Physische Geogr. 33, part A, 324 p., part B, 128 p.

MASARIK, J. 2002: Numerical simulation of in-situ production of cosmogenic nuclides. Geochim. Cosmochim. Acta 66 (15A), A491.

MASARIK, J., FRANK, M., SCHÄFER, J.M. & WIELER, R. 2001: Correction of in situ cosmogenic nuclide production rates for geomagnetic field intensity variations during the past 800,000 years. Geochim. Cosmochim. Acta 65, 2995–3003.

MCCABE, M.A. & CLARK, P.U. 1998: Ice-sheet variability around the North Atlantic Ocean during the last deglaciation. Nature 392, 373–377.

MIX A. C., BARD, E. & SCHNEIDER, R. 2001: Environmental processes of the Ice Age: land ocean glaciers (EPILOG). Quaternary Sci. Rev. 20, 627–657.

NIEDERMANN, S. 2000: The ^{21}Ne production rate in quartz revisited. Earth and Planet. Sci. Lett. 183, 361–364.

– 2002: Cosmic-ray-produced noble gases in terrestrial rocks: Dating tools for surface processes. In: PORCELLI, D., BALLENTINE, C. & WIELER, R. (Eds.). Noble Gases in Geochemistry and Cosmochemistry. Mineral. Soc. of Amer. 47, 731–784.

NIESSEN F., LISTER, G. & GIOVANOLI, F. 1992: Dust transport and paleoclimate during the Oldest Dryas in central Europe. Climate Dynamics 8, 71–81.

NUSSBAUM, F. 1910: Das Endmoränengebiet des Rhonegletschers von Wangen a. A. Mitt. naturf. Ges. Bern 1761, 141–168.

– 1951: Kenntniss der Eiszeitbildungen der Umgebung von Solothurn. Mitt. Naturf. Ges. Solothurn 16, 1–44.

OCHS, M. & IVY-OCHS, S. 1997: The chemical behavior of Be, Al, Fe, Ca, and Mg during AMS target preparation modeled with chemical speciation calculations. Nucl. Instr. Meth. B 123, 235–240.

PENCK, A. & BRÜCKNER, E. 1901/09: Die Alpen im Eiszeitalter, v. 1–3: Tauchnitz.

PHILLIPS, F.M., ZREDA, M.G., GOSSE, J.C., KLEIN, J., EVENSON, E.B., HALL, R.D., CHADWICK, O. A. & SHARMA, P. 1997: Cosmogenic ^{36}Cl and ^{10}Be ages of Quaternary glacial and fluvial deposits of the Wind River Range, Wyoming. Bull. Geol. Soc. Amer. 109, 1453–1463.

PHILLIPS, F.M., STONE W.D. & FABRYKA-MARTIN, J.T. 2001: An improved approach to calculating low-energy cosmic-ray neutron fluxes near the land/atmosphere interface. Chem. Geol. 175, 689–701.

PUTKONEN, J. & SWANSON, T. 2003: Accuracy of cosmogenic ages for moraines. Quaternary Res. 59, 255–261.

SCHLÜCHTER, C. 1988: The deglaciation of the Swiss Alps: A paleoclimatic event with chronological problems. Bull. Assoc. Franç. Etude Quaternaire 1988–2/3, 141–145.

SCHLÜCHTER, C. & RÖTHLISBERGER, C. 1995: 100,000 Jahre Gletschergeschichte. In: Gletscher im ständigen Wandel. Schweizerische Gletscherkommission, vdf Hochschulverlag AG an der ETH Zürich, 47–63.

SMALL, E.E., ANDERSON, R.S., REPKA, J.L. & FINKEL, R. 1997: Erosion rates of alpine bedrock summit surfaces deduced from in situ ^{10}Be and ^{26}Al. Earth and Planet. Sci. Lett. 150, 413–425.

STONE, J.O.H., ALLAN, G.L., FIFIELD, L.K. & CRESSWELL, R.G. 1996: Cosmogenic chlorine-36 from calcium spallation. Geochim. Cosmochim. Acta 60, 679–692.

STONE, J.O.H., EVANS, J.M., FIFIELD, L.K., ALLAN, G.L. & CRESSWELL, R.G. 1998: Cosmogenic chlorine-36 production in calcite by muons. Geochim. Cosmochim. Acta 62, 433–454.

STUIVER, M. & GROOTES, P.M. 2000: GISP2 oxygen isotope ratios. Quaternary Res. 53: 277–283.

STUIVER, M., REIMER, P.J., BARD, E., BECK, J.W., BURR, G.S., HUGHEN, K.A., KROMER, B., MCCORMAC, G., VAN DER PFLICHT, J., & SPURK, M. 1998: INTCAL98 radiocarbon age calibration, 24,000-0 cal B.P. Radiocarbon 40, 1041–1083.

SYNAL H.-A., BONANI, G., DÖBELI, M., ENDER, R.M., GARTENMANN, P., KUBIK, P.W., SCHNABEL, C. & SUTER M. 1997: Status report of the PSI/ETH AMS facility. Nucl. Instr. Meth. B 123, 62–68.

VAN HUSEN, D. 1997: LGM and Late-glacial fluctuations in the Eastern Alps. Quaternary Int. 38/39, 109–118.

– 2000: Geological processes during the Quaternary. Mitt. Österr. Geol. Ges. 92, 135–156.

WALKER, M.J.C., BJÖRCK, S., LOWE, J.J., CWYNAR, L.C., JOHNSEN, S., KNUDSEN, K.-L., & WOHLFARTH, B., INTIMATE Group. 1999: Isotopic 'events' in the GRIP ice core: a stratotype for the late Pleistocene. Quaternary Sci. Rev. 18, 1143–1150.

WELTEN, M. 1982: Pollenanalytische Untersuchungen im jüngeren Quartär des nördlichen Alpenvorlandes der Schweiz. Beitr. Geol. Karte der Schweiz NF 156, Stämpfli, Bern.

WESSELS, M. 1998 a: Late-Glacial and postglacial sediments in Lake Constance (Germany) and their palaeolimnological implications. Arch. Hydrobiol. Spec. Issues Advanc. Limnol. 53, 411–449.

– 1998 b: Natural environmental changes indicated by Late Glacial and Holocene sediments from Lake Constance, Germany. Palaeogeogr., Palaeoclimatogr., Palaeoecol. 140, 421–432.

WOHLFARTH, B., GAILLARD, M.-J., HÄBERLI, W. & KELTS, K. 1994: Environments and climate in southwestern Switzerland during the last termination 15–10 ka BP. Quaternary Sci. Rev. 13, 361–394.

YOKOYAMA, Y., LAMBECK, K., DE DECKER, P., JOHNSTON, P. & FIFIELD, L.K. 2000: Timing of the Last Glacial Maximum from observed sea-level minima. Nature 406, 713–716.

ZARAGOSI, S., EYNAUD, F., PUJOL, C., AUFFRET, G.A., TURON, J.L. & GARLAN, T. 2001: Initiation of the European deglaciation as recorded in the northwestern Bay of Biscay slope environments (Meriadzek Terrace and Trevelyan Escarpment): a multi-proxy approach. Earth and Planet. Sci. Lett. 188, 493–507.

ZREDA, M. & PHILLIPS, F.M. 1995: Insights into alpine moraine development from cosmogenic ^{36}Cl buildup dating. Geomorph. 14, 149–156.

ZREDA, M. G. 1994: Development and calibration of the ^{36}Cl surface exposure dating method and its application to the chronology of Late Quaternary glaciations. Ph.D. diss., New Mexico Institute of Mining and Technology, Socorro, 318 p.

Manuscript received May 28, 2003
Revision accepted January 14, 2004